

Quantitative Method of Image Analysis when Drift is Present in a Scanning Probe Microscope

S. H. Huerth¹ and H. D. Hallen
North Carolina State University
Raleigh, NC 27695

Abstract

We present a quantitative method of image analysis that automatically corrects for system drift in comparisons of images before and after an event under study. The method utilizes 2-dimensional correlations followed by automatic z-scaling, shifting, and the calculation of a difference image from the before and after images. Optical reflectance near-field scanning optical microscope (NSOM) images that show the effects of oxygen electromigration are used as an example system. The tunnel current that induces the atomic motion is provided by the metallic NSOM aperture in a scanning tunneling microscope (STM) mode. The analyzed (difference) image clearly shows the effects that are otherwise obscured by native oxygen concentration variations, demonstrating the utility of the method. The related issues of false positive/negative probabilities for given noise levels and thresholds are also discussed.

PACS Numbers:
07.05.Kf, 07.05.Pj, 07.79.-v, 78.67.-n, 66.30.Qa

Introduction

Scanned probe microscopies provide nanometric data such as topography, [1] fluorescence, [2-4] spectroscopy [5-9] and reflectance. [10] A drawback is that these

proximal probe microscopes tend to be slow when used in the more powerful contrast modes, due to signal averaging, which increases the image-time required when quantifying changes due to time or processing. Data analysis to quantify a change requires comparison of the before and after images. We present here a correlation-based automatic method for accurately identifying relative image positions and then comparing the images. Since accurate relative positioning of images is used primarily to test for a change between the images, we present a discussion of the statistics of detecting such changes.

The inherent drift in scanning probe microscopy makes the comparison of sequential images difficult. Drift is the gradual system movement over time primarily due to changes in temperature. Most microscopes are covered and many are insulated to reduce drift to ~ 100 nm/hr. The microscope system may be placed in a temperature-controlled environment if more stability is required, but this is expensive and difficult. Therefore, to be able to compare images, the drift must be calculated and one image shifted with respect to the other so that the area of overlap is compared. Processing of the sample can involve a significant amount of time that allows drift to become important. For example, electromigration of oxygen in Yttrium barium cuprate ($\text{YBa}_2\text{Cu}_3\text{O}_{7.8}$ or YBCO) by injection of tunnel electrons can take more than 30 minutes. [11, 12] Studies of surface diffusion at high resolution are also sensitive to drift due to the small length scales. To eliminate possible bias, one would prefer the method for calculating drift to not require tweaking by an operator. We present such a quantitative method of image

¹ Current address: Microelectronics Center of North Carolina, Research Triangle Park, NC

analysis that corrects for system drift, allowing automatic comparison of the before and after images. A related topic that usually arises when comparing before and after images is whether or not there is an effect at all. We discuss this in relation to the method and scanning proximal probe data.

Methods

The analysis of the images can be broken down into several major tasks: (1) identification of the shift between the before and after images. When the proximal probe produces both a topographic and another image such as an optical (NSOM), phase (tapping AFM), or other contrast mode image, the drift can be measured on the topographic image. This is especially useful if the image that changes is the non-topographic image, as it permits an independent verification that the topography did not change. Such verifications can eliminate artifacts due to, e.g., tip damage during the sample modification. (2) adjustment of the z-scaling of the before and after images due to calibration changes or tip wear. Laser drift in NSOM, or preamplifier drift in almost any of the microscopes contributes to the need for this step. (3) Subtraction and analysis of the significance of a measured effect. Usually the type of expected changes (diffusion along an observed contrast line or the creation of a new feature in the image) are known qualitatively a-priori. Tip wear can cause derivative-like features in the subtracted image that mask the changes. If this is excessive, then the before image can be filtered to reduce its resolution. Noise in the images can also mask changes. This can be analyzed and appropriate thresholds chosen for identifying weak effects without causing excessive false positives.

The 2-dimensional correlation function is used to identify shifts between the before and after images. This statistical technique involves shifting one image with respect to another, multiplying, and adding. It works best when the data vary reasonable rapidly about zero throughout the image, so that the positive and negative values tend to cancel to give zero except when the images are properly aligned (no relative drift). We have found that topographic images of granular materials meet this requirement well. It often helps to subtract a least-squares fit plane from the data to bring the average value towards zero, but we do not find it necessary in general. For weak optical data [11, 12] or scanning Hall probe data, [13-15] we have found that scan-line noise can be problematic. The scan-line noise is due to ‘switching’ noise in the detector background or gain (or defects changing state in the sub-micron Hall probe) with a time constant similar to or longer than the time to scan one line. The switching noise dominates the $1/f$ noise in these systems. It appears as abrupt shifts in the signal level. Its statistical nature implies that it will not correlate from image to image. We have used two methods that can control the noise when the $1/f$ noise cannot be eliminated by experimental schemes: (1) z-scaling each line of the image so that all the line sums are identical, or (2) stretching the image data into a one-dimensional array versus time, finding the jumps in the data due to switching noise, and removing them by offsetting the data after the switch. The former is popular in commercial instruments and works well for images with several regions of contrast throughout the image. It can produce artifacts such as adding contrast to an otherwise flat background when these assumptions are not met, for example, it will add contrast to the background if the true image were a flat background with a large bright

region in the center of the image. The latter requires that the steps up and down of the switching noise are all of nearly equal height (met in many cases), and also requires that the sample contrast not have sharp features that could be removed inadvertently. The appropriate method will vary with the application. Our advice is to use the topography, which usually does not suffer from such problems, and take other data in such a way as to minimize the scan-line noise (do not run at too high a PMT gain, watch detector bias, etc.).

The correlation is computed using the fast Fourier transform. [16] This assumes a periodic function, which we do not have, so the image is zero-padded to double the number of points in each direction. The fast Fourier transform (FFT) of the before $\mathcal{F}_{\text{before}}$ and after $\mathcal{F}_{\text{after}}$ images are multiplied, and the inverse transform computed $c(x,y) = \mathcal{F}^{-1}(\mathcal{F}_{\text{after}} * \mathcal{F}_{\text{before}}^*)$, where the before image transform has been complex-conjugated. Most commercial data acquisition and analysis packages such as LabView, MatLab, IDL and others have routines available for computing fast fourier transforms and often correlations. Algorithms can also be found in books such as [Press, 1986 #734] and in software libraries on the web. What we do next, scale by the number of nonzero points used in the calculation of each point, is required since we zero-pad the image, but is usually not found in the standard packages. We now scale $c(x,y)$ by the number of overlapping image points – for a shift of (i,j) , the scale factor is $(N_x - |i|) * (N_y - |j|)$ -- to obtain the correlation $C(x,y)$, where $N_{x(y)}$ is the number of image points in x (y). Most FFT algorithms put the $(0, 0)$ shift element at the $(0, 0)$ array location of $C(x,y)$, and the shifts with small negative i or j at the corners of this $(2N_x$ by $2N_y)$ array. We reorganize

to position the (0,0) shift in the center of the array, and reduce the size of $C(x,y)$ to an (N_x by N_y) array with shifts from $(-N_x/2, -N_y/2)$ to $(N_x/2-1, N_y/2-1)$. This choice of a subset of the correlation assumes that the image has drifted by less than half its size, and is made to provide a reasonable numbers of overlap points in the calculation of the correlation C for every point in the final array. The shift (drift) between the before and after images is taken to be the shift corresponding to the maximum value of C . We have found that C is usually sharply peaked, making this identification straightforward and trustworthy. Examples for very different looking topographies are shown in Figs. 1 and 2. Before and after topographies are shown along with the corresponding correlations C . In Fig. 1, a 256x256 pixel image, the correlation function peak position implies that the x position had moved 55 pixels left and the y position had moved 56 pixels up. In terms of drift, this is -1078nm and 1098 nm down in 5.38 hours (several images at different wavelengths were taken between) for a drift of 286 nm/hour. For Fig. 2, 128x128 pixels, the -30, 40 nm shift in 57 min. gives 53 nm/hr drift. The actual shifted/z-scaled and subtracted image is also shown in the figure with the same gray range as the before and after images.

As noted above, the before image is scaled in the z- or optical-direction and shifted in the x and y directions before being subtracted from the after image to form a difference image. The z-scale is usually chosen to minimize the sum of $\{(the\ after\ image) - z-scale*(the\ shifted\ before\ image)\}^2$ over the points in the overlapping region of the images, utilizing the calculated shift values. We have also used a z-scale factor given by the ratio of the center values of the image color scales when the z-scale ranges are set to

be identical while the z-scales are offset with respect to each other until the images look similar. This latter method works very well, but requires operator intervention. The z-scale is set to 1 in the topographic difference image shown in Fig. 1 since there is no reason for the topography to become uncalibrated, but our optical data frequently needs a small, few percent, correction.

The method was programmed in c and inserted into a code interface node (CIN) of the LabView programming environment.

Examples

As an example of the method for analyzing optical data from a NSOM microscope, we show data relating to studies of oxygen electromigration in YBCO. Two figures show data from two samples prepared by different growth techniques, [12] and electromigrated with the NSOM-based system. White corresponds to higher topography or larger local oxygen content in the images. Even though the topographic images have a different qualitative structure, they both produce correlations with well-defined, single peaks, that represent an image shift of $(dx, dy) = (-55, 56)$ pixels (of 256 square) in Fig. 1(c), and $(dx, dy) = (-3, 4)$ pixels (of 128 square) in Fig. 2(c). The analysis of the changes due to injected electrons is complicated by the large native variations in oxygen content with position, Figs. 1&2 (d). These can completely swamp any induced changes, as can be seen by comparing the before and after optical images in Fig. 1. The difference images, Figs. 1&2 (f), clearly show the effects, however, and guide one to find the subtle differences that do exist in the before and after images. An oxygen increase is observed

in both cases where the EIM occurred. In both cases, the ‘before’ image is the one that is shifted, so direct comparison of the data at a given image position should be made to the ‘after’ data. Images of the Fig.1 data with arrows to show the relative positions are in [12]. The region of increased oxygen content in Fig. 1 lies within one grain. The shift-scale-subtracted image, Fig. 1(f), can be used to make this obvious. We first create a contour image corresponding to Fig. 1(f) then overlay it on Fig. 1(b), the ‘after’ topography. This is shown in Fig. 3. The nearly circular contours indicate the grain in which the oxygen content increased. It is not obvious where the oxygen came from to fill the grain shown in Fig. 1(f),3. Presumably it came from the bulk of the film, below the depth-sensitivity of the instrument, or uniformly around the grain such that the change in contrast at any one point is below the noise level. This is not the case in the data of Fig. 2. An obvious region of oxygen content decrease is also seen in the figure. We found that the electrons enhance diffusion, so the source of oxygen is expected to vary strongly with the oxygen distribution before the experiment. When it is visible, it often is connected to the EIM region via a grain boundary, indicating that oxygen easily diffuses along (but not necessarily through) grain boundaries. Another example of the image processing technique is shown in Fig. 4. In this case, we were checking whether or not the laser light used to image the oxygen concentration could induce oxygen motion. In this case, a shift $(dx, dy) = (-2, 4)$ pixels (of 128 square) and a z-scaling of the initial image by a factor 1.19 was required for the shift-scale-subtraction. The regions of non-overlap are set to zero, and can be seen as thin gray regions along two sides of the image. As expected, no obvious changes are observed. This indicates that the electrons are required for the effect.

False Positive/Negative Analysis

When analyzing the output of the shift/scale subtract, it is important to know when there is and when this is not a real effect. We consider two approaches to this problem. The first uses a threshold. A positive is assumed when N contiguous points exceed the threshold value y_{th} . The second method compares the mean value of the region of suspected effect before and after the experiment. The former has the advantage of simplicity and ease of implementation in a scanning probe microscope environment. The latter can make use of the readily available student's t -test, and can work well when an effect is observed, but is hard to implement to determine a negative result unless the size of the effect is known a-priori.

When using the threshold method, we can estimate the probability of missing an effect (false negative) or of a false positive. This will be determined by the signal to noise ratio, the number of points in the region of the possible effect, N , and the threshold, y_{th} , used to identify an effect. We can measure the noise level from a difference image taken where and when no effect should be observed. The standard deviation of any single data point σ_{perpt} is given by the square root of the calculated variance. [17] We assume in the analysis that the noise has a Gaussian distribution. The threshold and N (lateral size of the effect) can be determined by extrapolation from other data when the effects are obvious. The threshold is then selected with consideration of the noise in conjunction with the expected signal levels (also extrapolated from data with strong effects or modeling). For a noise level (per point) characterized by a standard deviation σ_{perpt} , the probability that all the points in a region of size N exceed the threshold (a false

positive in a particular place) is given by the integral of the tail of a Gaussian with standard deviation $\sigma = \sigma_{\text{perpt}} / \sqrt{N}$, from $(y_{\text{th}} - y_{\text{ave}})$ to ∞ , the complementary error function

$$\frac{1}{2} \operatorname{erfc}\left(\frac{y_{\text{th}} - y_{\text{ave}}}{\sqrt{2} \sigma}\right), \quad (1)$$

[18] where we have assumed a positive signal. The background signal level is y_{ave} , and the \sqrt{N} scaling of the standard deviation assumes that the noise is independent. To insure independent samples, the time constants of the image acquisition must be faster than the scan rate. The probability of a false negative when the effect is of size N and the signal level is y_{sig} (assume positive) is $\frac{1}{2} \operatorname{erfc}\left(\frac{y_{\text{sig}} - y_{\text{th}}}{\sqrt{2} \sigma}\right)$, which is 50% if $y_{\text{sig}} = y_{\text{th}}$, approaches zero as y_{sig} increases, and approaches 1 as y_{sig} decreases.

For our examples, we measure the noise from the histograms of the background regions. Some of these are shown in Fig. 5. These background histograms resemble Gaussians. The standard deviations of the noise evident from the figures is 0.06 for the Fig. 2 data from Fig. 5(a), 0.07 for the Fig. 4 data from Fig. 5(b), and 0.44 for the Fig. 1 data (histogram not shown, but similar to others). If we use a threshold value of $y_{\text{th}} = 16$ a.u. in the Fig. 1(f) data, which corresponds to a value 4 single-point standard deviations, $\sigma_{\text{perpt}} = \sigma * \sqrt{N}$, above the background average y_{ave} , we find that there are ~ 500 contiguous points above the threshold, so the threshold is $4 * \sqrt{500}$ σ 's above threshold. The probability of a false negative in the Fig. 1 data, Eqn. 1, is essentially zero ($< 10^{-1000}$), primarily due to the large number of points. If we use a threshold value of $y_{\text{th}} = 0.1$ a.u. in the Fig. 2(f) data, which corresponds to a value 1.67 single point standard deviations

above the background average y_{ave} , we find that there are ~ 1500 contiguous points above the threshold. The probability of a false negative in the Fig. 1 data is also ~ 0 . An estimate of the probability of a false negative for a known region of modest size $N=100$ points in a known location for the Fig. 4 data will be presented next. If we choose a threshold $y_{th} = 0.1$, note that $y_{ave} = 0.06$ for the data in Fig. 4, and assume the signal value for a positive here would be 0.12, then $y_{sig} - y_{th} = 0.02/0.07*\sqrt{100}*\sigma$, and the probability of a false negative is $0.5*erfc(\sqrt{2} / .7) = 0.0021$.

The alternative method to test for a change in the image is to abandon the use of a threshold to signal a change, but instead compare the means in the region where an effect is expected. This is done using the student's t-test [Press, 1986 #734]. The output of the t-test is $A(t, \nu) = 1 -$ (the probability that the means would be this different by chance), given the number of degrees of freedom ν and the t-value t . If we compare the mean $\langle y \rangle$ of the region of the image containing N points before and after stressing the sample, and assume that the noise level remains fixed (with standard deviation σ , as we have

observed to be the case), then $t = \sqrt{\frac{N}{2}} \frac{\langle y \rangle_{after} - \langle y \rangle_{before}}{\sigma}$ and $\nu = 2(N-1)$. The factor multiplying the difference of the means is the inverse of the standard error of the two measurements. Now $A(t, \nu) = 1 - I_{\nu/(\nu+t^2)}(\nu/2, 0.5)$, with I the incomplete beta function, is roughly the probability that the means are different. We now proceed to re-analyze the data in figures 1, 2, and 4. For Fig, 1, we find that $\langle y \rangle_{after} = 19.2$, $\langle y \rangle_{before} = 14.3$ and $\sigma = 0.44$ for before and after, from histograms of the $N = \sim 500$ point region. This gives $A(t, \nu) = 1 - (<10^{-1000})$, similar to what we found above. If just the center of the region is used,

with 100 points, then $A(t, \nu) = 1 - 2 \times 10^{-157}$, which shows that the large number of points is what makes the effect so obvious. For the Fig, 2 data, $\langle y \rangle_{\text{after}} = 2.54$, $\langle y \rangle_{\text{before}} = 2.37$ and $\sigma = 0.06$ both before and after, in the $N = \sim 1500$ point region. This gives $A(t, \nu) = 1$. There is no obvious effect for Fig. 4. Thus we do not know the number of points to compare. This shows the benefit of the threshold approach. What one can say in general, however, is that if the difference in the means is one-half a standard deviation and the number of points that we compare is 100, then the function $A(t, \nu) = 1 - 5 \times 10^{-4}$. We see that the results of this analysis are comparable to those given above – the qualitative meaning and order of magnitude is similar although the exact meaning of the calculated quantities differs.

There are some non-statistical effects that deserve comment. In the image analysis with which we are concerned here, the primary sources are (1) improper z-scaling, (2) improper shifting of the before image, (3) resolution changes, and (4) scan-line noise. The last source requires better data, or can be treated as statistical noise if there are enough data points in the expected affected region. Sources (2) and (3) result in derivative-like features in the image, so are observed as edge-enhancements on one or all sides of features, respectively. They tend to form lines rather than areas, so would likely not cause false positives or negatives. Source (1) can be evaluated in regions far from those where an effect is anticipated. Since these can cause false positives, use of the maximum in those regions for y_{ave} will provide the most conservative estimate of the false positive probability. We also note that this analysis has assumed that the affected region is known, as it would be when the tip is used to cause an effect. In some cases, this may

not be true, or may be only approximately true. Then, one must multiply the above results by the number of possible configurations of points of the given N in the region of possible effect, with appropriate constraints. Since this number can be quite large (resulting in part from a factorial or binomial coefficients), the probabilities for false results is much larger than for those noted above.

Conclusions

A 2-d correlation between sequential scanned probed images can be used to determine the systematic drift. The drift then can be used to compare the images for changes due to some effect being studied. This proved useful for the extraction of oxygen electromigration information from NSOM images that were dominated by native oxygen concentration variations. A statistical analysis of the difference data was given to determine if the observed effect is significant.

Acknowledgements

This work was supported by the Office of Naval Research through grant N00014-98-1-0228 and the National Science Foundation through grant DMR-9975543

References

- [1] E. Betzig and J.K. Trautman, "Near-field optics: Microscopy, spectroscopy, and surface modification beyond the diffraction limit," *Science* **257**, 189 (1992).
- [2] Randy X. Bain, Robert C. Dunn, X. Sunney Xie and P.T. Leung, "Single Molecule Emission Characteristics in Near-Field Microscopy," *Phys. Rev. Lett.* **75**, 4772 (1995).
- [3] Eric Betzig and Robert J. Chichester, "Single Molecules Observed by Near-Field Scanning Optical Microscopy," *Science* **262**, 1422 (1993).
- [4] X. Sunney Xie and Robert C. Dunn, "Probing Single Molecule Dynamics," *Science* **265**, 361 (1994).
- [5] C.L. Jahncke, M.A. Paesler and H.D. Hallen, "Raman imaging with near-field scanning optical microscopy," *Appl. Phys. Lett.* **67**, 2483 (1995).
- [6] R. D. Grober, T. D. Harris, J. K. Trautman, E. Betzig, W. Wegscheider, C.L. Pfeiffer and K. West, "Optical spectroscopy of a GaAs/AlGaAs quantum wire structure using near-field scanning optical microscopy," *Appl. Phys. Lett.* **64**, 1421 (1994).
- [7] H. F. Hess, E. Betzig, T. D. Harris, L. N. Pfeiffer and K. W. West, "Near-field spectroscopy of the quantum constituents of a luminescent system," *Science* **266**, 1740 (1994).
- [8] E. J. Ayars, H. D. Hallen and C. L. Jahncke, "Electric field gradient effects in Raman spectroscopy," *Phys. Rev. Lett.* **85**, 4180 (2000).
- [9] E.J. Ayars and H.D. Hallen, "Surface enhancement in near-field Raman spectroscopy," *Appl. Phys. Lett.* **76**, 3911 (2000).
- [10] M.A. Paesler and P.J. Moyer, "Near-Field Optics: Theory, Instrumentation and Applications," (John Wiley and Sons, Inc., New York, 1996).

- [11] Suzanne Huerth, Michael Taylor, Michael Paesler and Hans Hallen, "Near-Field Scanning Optical Microscopy of Electromigration in YBCO," Proceedings of the Second Asia-Pacific Workshop on Near-field Optics, Beijing, China, (1999).
- [12] S. H. Huerth, M. P. Taylor, H. D. Hallen and B. H. Moeckly, "Electromigration in YBCO using a Metal Clad Near-Field Scanning Optical Microscope Probe," Appl. Phys. Lett. **77**, 2127 (2000).
- [13] A.M. Chang, H.D. Hallen, H.F. Hess, H.L. Kao, J. Kwo, R. Wolf, J. van der Zeil and T.Y. Chang, "Scanning Hall probe microscopy," Appl Phys. Lett. **61**, 1974 (1992).
- [14] A.M. Chang, H.D. Hallen, H.F. Hess, H.L. Kao, J. Kwo, A. Sudbø and T.Y. Chang, "Scanning Hall probe microscopy of a vortex and field fluctuations in $\text{La}_{1.85}\text{Sr}_{0.15}\text{CuO}_4$ films," Europhys. Lett. **20**, 645 (1992).
- [15] H.D. Hallen, R. Seshadri, A.M. Chang, R. Miller, L.N. Pfeiffer, K. West, C.A. Murray and H. F. Hess, "Direct spatial imaging of vortices in a superconducting wire network," Phys. Rev. Lett. **71**, 3007 (1993).
- [16] William H. Press, Brian P. Flannery, Saul A. Teukolsky and William T. Vetterling, "Numerical Recipes," (Cambridge University Press, Cambridge, 1986).
- [17] Philip R. Bevington and D. Keith Robinson, "Data reduction and error analysis for the physical sciences," (McGraw-Hill, New York, 1992).
- [18] Milton Abramowitz and Irene A. Stegun, "Handbook of mathematical functions, with formulas, graphs, and mathematical tables," (National Bureau of Standards, U.S. G.P.O., Washington, D.C., 1981).

Figure Captions

Figure 1.

Images of a YBCO film made by laser ablation. All are 5 micron square (-2500 -> 2500 nm) except (f), which is a subset of the area (x: -2500 -> 1400, y: -1400 -> 1500). (a) The topography before electromigration. The white areas are higher in this 150 nm gray-range image. (b) The topography after, also with a 150 nm gray range. (c) The correlation image, with gray range -25 -> 35. The whiter area is more correlated, and zero relative shift is at the center. (d) the optical image before electromigration. The whiter regions correspond to a higher oxygen content on this 177 -> 187 a.u. gray range. (e) The optical image after EIM, with 200 -> 212 a.u. gray range. (f) The shifted-scaled-subtracted image from (e) minus a shifted and z-scaled (d). The whiter region shows the increase in oxygen where the EIM was performed with gray range 10 -> 22 a.u.

Figure 2.

Images of a YBCO film made by co-evaporation. All are 1270 nm square. (a) The topography before electromigration. The white areas are higher in this 330 nm gray-range image. (b) The topography after, with the same gray range as before. (c) The correlation image, with gray range -750 -> 1250. The whiter area is more correlated, and zero relative shift is at the center. (d) the optical image before electromigration. The whiter regions correspond to a higher oxygen content on this 12.8 -> 13.4 a.u. gray range. (e) The optical image after EIM, with 12.5 -> 13.1 a.u. gray range. (f) The shifted-

scaled-subtracted image from (e) minus a shifted and z-scaled (d). The whiter region shows the increase in oxygen where the EIM was performed with gray range 2 -> 2.6 a.u.

Figure 3.

The region of Fig. 1(b) corresponding to that of Fig. 1(f) is plotted as a gray scale with white signifying a higher topography. The data of Fig. 1(f) has been converted to a contour image and overlaid. The black circles over the grain near the top center encircle the region of increased oxygen content in Fig. 1(f). The other circled regions are of much smaller variations in the shift-scaled-subtracted image, and may be due to noise.

Figure 4.

A 1530 nm square region of YBCO grown by co-evaporation is shown. (a) the shift-scaled-subtracted optical image with 1 a.u. gray range shows no apparent structures due to laser illumination. (b) The after optical image with gray range 8.1 -> 9.1 a.u., for comparison, shows large regions of native oxygen concentration variations.

Figure 5.

Histograms of the shift-scale-subtract data from figures 2 and 3. In both cases, the spikes at value = 0 are due to setting the image points in the non-overlap region to zero, hence should be ignored. (a) Histogram from the region in Fig. 2(f) where there were no obvious changes, the background in the upper part of the image. (b) A histogram of the all the data in Fig. 3(a).

Figure 1 of 5, Huerth and Hallen, “Quantitative Method of Image Analysis when Drift is Present in a Scanning Probe Microscope”

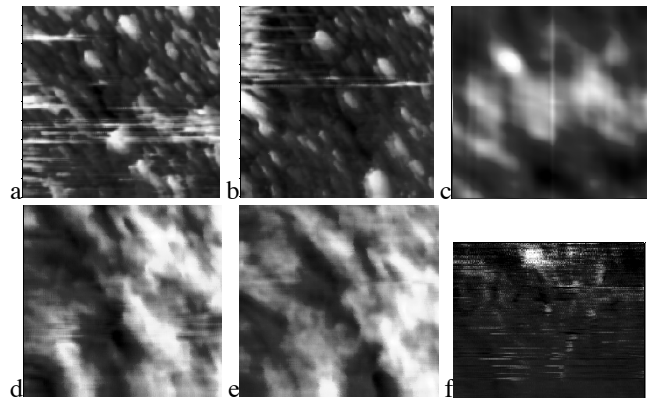


Figure 2 of 5, Huerth and Hallen, “Quantitative Method of Image Analysis when Drift is Present in a Scanning Probe Microscope”

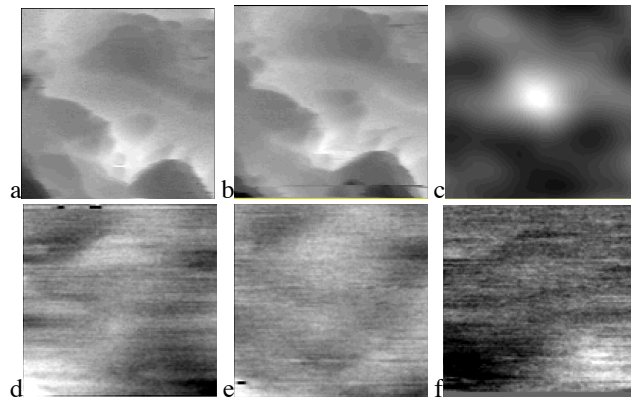


Figure 3 of 5, Huerth and Hallen, "Quantitative Method of Image Analysis when Drift is Present in a Scanning Probe Microscope"

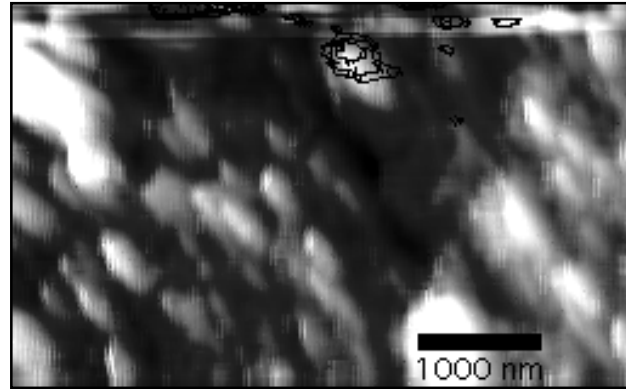


Figure 4 of 5, Huerth and Hallen, “Quantitative Method of Image Analysis when Drift is Present in a Scanning Probe Microscope”

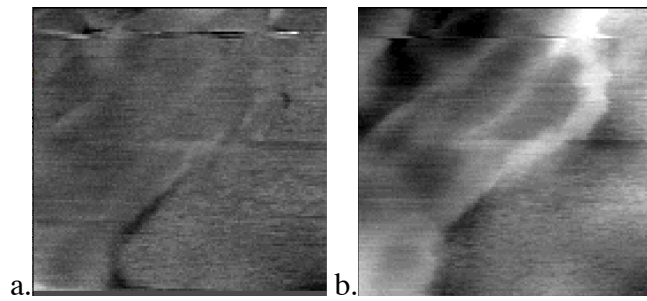


Figure 5 of 5, Huerth and Hallen, “Quantitative Method of Image Analysis when Drift is Present in a Scanning Probe Microscope”

